Molybdenum(V) Sites in Xanthine Oxidase and Relevant Analogue Complexes: Comparison of Molybdenum-95 and Sulfur-33 Hyperfine Coupling

Graham L. Wilson,[1a,b] Richard J. Greenwood,[1a] John R. Pilbrow,[1b] Jack T. Spence,[1c] and Anthony G. Wedd*[,1a,d]

Contribution from the Department of Chemistry, La Trobe University, Bundoora, Victoria 3083, Australia, Department of Physics, Monash University, Clayton, Victoria 3168, Australia, and Department of Chemistry and Biochemistry, Utah State University, Logan, Utah 84322-0300.
Received November 19, 1990

Abstract: ^{95}Mo ($I = {}^5/_2$) hyperfine matrices have been defined from multifrequency (2-4 and 9 GHz) electron spin resonance spectra of the Rapid Type 1, Rapid Type 2, and Slow centers of milk xanthine oxidase. For comparison, ^{95}Mo hyperfine matrices were similarly extracted for the synthetic species $[MoOXL]^-$ and $[MoO(XH)L]$ (X = O, S; LH_2 = *N,N'*-dimethyl-*N,N'*-bis(2-mercaptophenyl)-1,2-diaminoethane). In addition, ^{33}S ($I = {}^3/_2$) hyperfine matrices were derived for the thio ligand of $[MoOSL]^-$ and for the mercapto ligand SH of $[MoO(SH)L]$ for comparison with the ^{33}S coupling observed in a number of EPR signals of xanthine oxidase. Detailed examination confirms $[Mo^VO(SH)]$, $[Mo^VO(SH)(OH)]$, and $[Mo^VO(OH)]$ as the centers responsible for the Rapid Type 1, Rapid Type 2, and Slow EPR signals and provides compelling evidence that $[Mo^VOS]$ is the source of the Very Rapid signal. A characteristic of the catalysis is a correlated electron-proton transfer from substrate to the molybdenum site. The present work suggests a specific mechanism: reduction of the $Mo^{VI}OS$ resting form to Mo^V or Mo^{IV} causes occupation of a highly covalent MoS π-antibonding orbital with a consequent increase in the basicity of the thio ligand.

Introduction

The molybdenum hydroxylase or oxomolybdenum enzymes[2,3] catalyze a variety of two-electron redox reactions. A common feature may be a primary oxo transfer step.[4,5] In the xanthine oxidase/dehydrogenase systems (XnO/XnD), correlated electron-proton transfer from substrate to the molybdenum site is another aspect. Stoichiometrically, oxidation of substrate RH may be written as formal insertion of an oxygen atom into a CH bond:

$$RH + [O] \rightarrow ROH$$

$$RH + H_2O \rightarrow ROH + 2H^+ + 2e^-$$

Each enzyme features a pterin unit closely associated with the molybdenum atom (the molybdenum cofactor),[6,7] and in the great majority of cases an internal electron transfer chain connects formal oxidizing and reducing sites. During turnover, the molybdenum sites cycle through oxidation states VI, V, and IV. The most direct structural information comes from EXAFS measurements.[8-10] These indicate the presence of a $[Mo^{VI}OS(SR)_2]$ unit in the resting active forms of XnO/XnD and $[Mo^{VI}O_2(SR)_{2\text{ or }3}]$ in the inactive "desulfo" forms. A single oxo ligand is detected in the Mo^{IV} forms.

Scheme I[a]

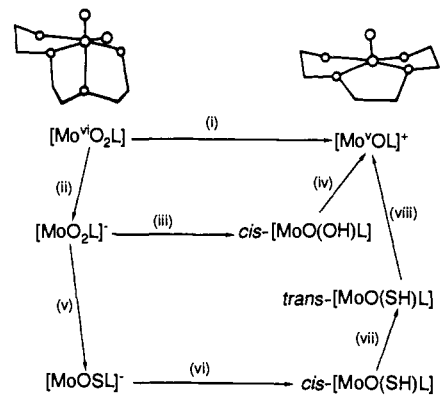

[a] Key: (i) e^-, $2H^+$, $-H_2O$; (ii) e^- or SH^-, 25 °C; (iii) H^+, -40 °C; (iv) H^+, $-H_2O$; 25 °C; (v) SH^-, 25 °C; (vi) H^+, -78 °C; (vii) 0 °C; (vii) H^+, $-H_2S$, 25 °C.

Electron paramagnetic resonance (EPR) signals characteristic of Mo^V appear upon reduction of the enzymes.[11-13] In particular, the Very Rapid ($t_{1/2} \approx 10$ ms) and Rapid Type 1 ($t_{1/2} \approx 25$ ms) signals are implicated with turnover of active XnO by xanthine and related substrates. The Slow signal appears upon reduction of desulfo XnO by dithionite. Bray's prolific work[11-13] has provided a wealth of EPR information at 9- and 35-GHz frequencies which includes ^1H, ^{13}C, ^{17}O, ^{33}S, and ^{95}Mo hyperfine coupling data for atoms associated with the catalysis.

Note that naturally occurring molbdenum contains nuclei that are both nonmagnetic ($I = 0$; 74.82 atom %) and magnetic (^{95}Mo: $I = {}^5/_2$, 15.72 atom %, $\mu = -0.9133\ \beta_N$. ^{97}Mo: $I = {}^5/_2$, 9.46 atom %, $\mu = -0.9235\ \beta_N$). Consequently, each anisotropic component of the EPR spectrum exhibits the characteristic pattern of an intense central resonance flanked by six weak hyperfine resonances.

(1) (a) La Trobe University. (b) Monash University. (c) Utah State University. (d) Present address: School of Chemistry, University of Melbourne, Victoria, 3052, Australia.
(2) Spiro, T. G. Ed. *Molybdenum Enzymes*; John Wiley: New York, 1985.
(3) Coughlan, M. P., Ed. *Molybdenum and Molybdenum-containing Enzymes*; Pergamon Press: Oxford, New York, 1980.
(4) Hille, R.; Sprecher, H. *J. Biol. Chem.* **1987**, *262*, 10914-10917.
(5) Holm, R. *Coord. Chem. Rev.* **1990**, *110*, 183-221.
(6) (a) Johnson, J. L.; Bastian, N. R.; Rajagopalan, K. V. *Proc. Natl. Acad. Sci. U.S.A.* **1990**, *87*, 3190-3194. (b) Taylor, E. C.; Ray, P. S.; Darwish, I. S.; Johnson, J. L.; Rajagopalan, K. V. *J. Am. Chem. Soc.* **1989**, *111*, 7664-7665 and references therein. (c) Gardlik, S.; Rajagopalan, K. V. *J. Biol. Chem.* **1990**, *265*, 13047-13054.
(7) Cramer, S. P.; Stiefel, E. I. In ref 2, pp 411-441.
(8) Cramer, S. P. *Adv. Inorg. Bioinorg. Mech.* **1983**, *2*, 259.
(9) (a) Hille, R.; George, G. N.; Eidness, M. K.; Cramer, S. P. *Inorg. Chem.* **1989**, *28*, 4018-4022. (b) Turner, N. A.; Bray, R. C.; Diakun, G. P. *Biochem. J.* **1989**, *26*, 563-571.
(10) George, G. N.; Cleland, W. E., Jr.; Enemark, J. H.; Smith, B. E.; Kipke, C. A.; Roberts, S. A.; Cramer, S. P. *J. Am. Chem. Soc.* **1990**, *112*, 2541-2548.
(11) George, G. N.; Bray, R. C. *Biochem. Soc. Trans.* **1987**, *13*, 570-567 and references therein.
(12) Bray, R. C. *Q. Rev. Biophys.* **1988**, *21*, 299.
(13) George, G. N.; Bray, R. C. *Biochemistry* **1988**, *27*, 3603-3609.

0002-7863/91/1513-6803$02.50/0

The individual ^{95}Mo and ^{97}Mo features are normally not resolved.

Spectroscopic models that assist with molecular interpretation of the enzyme EPR signals have been generated recently.[14-18] When most *cis*-[$Mo^{VI}O_2$] complexes undergo reductive electrolysis, H_2O is eliminated, producing [$Mo^{V}O$], [$Mo^{V}_2O_3$], or [$Mo^{IV}O$] species. For a number of quadridentate ligands with N_2S_2 or N_2O_2 donor sets,[14-16,19] steric barriers appear to disfavor the ligand conformational change normal for conversion of *cis*-[$Mo^{VI}O_2$] to [$Mo^{V}O$] centers (Scheme I). Consequently, a number of intermediates can be intercepted along the reaction pathway, and clean chemistry is observed for the ligand LH_2 = *N,N'*-dimethyl-*N,N'*-bis(2-mercaptophenyl)-1,2-diaminoethane (Scheme I).

Structural assignments rest upon observed EPR parameters (^{1}H and ^{17}O hyperfine coupling constants, in particular)[14,16,17] and the comparitive properties of Ph_4P[MoOSL], *trans*-[MoO(SH)L], and *cis*-[$MoO(OSiMe_3)$L] isolated in substance.[17,18] X-ray structural confirmation is available for the latter compound only. In the thio system, the cis–trans isomerization of [MoO(SH)L] (Scheme I, step vii) appears to be the step slowed by the ligand conformational barrier.

Comparison of average coupling constants $a(^1H)$ and $a(^{17}O)$ of the analogue compounds with enzyme data is consistent with *cis*-[$Mo^{V}O$(SH)] and *cis*-[$Mo^{V}O$(OH)] centers being responsible for the Rapid Type 1 and Slow signals of XnO, respectively.[14,16,17] However, the nature of the Very Rapid signal has not been so clear-cut.[11-13,16,17] The signal is characterized by a high g_z value (>2.02), by reduced A(^{95}Mo) components compared to the Rapid signals, and particularly, by highly anisotropic coupling to a single ^{33}S atom.[13,20,53]

Improved resolution of EPR spectra in both liquid and frozen solution at lower frequencies (2–4 GHz) has been observed for Mo^{V}, W^{V}, and Cu^{II} complexes and for some Cu^{II} proteins.[21] The prospect of improved resolution of the various hyperfine couplings seen in XnO spectra was an important incentive for the present work. While this was not realized, multifrequency spectra have allowed extraction of the ^{95}Mo ($I = {}^5/_2$) hyperfine matrices for the Rapid Type 1, Rapid Type 2, and Slow signals of XnO to complement those derived previously for the Very Rapid and Rapid Type 1 signals.[13] For comparison, ^{95}Mo matrices have been defined for the species [MoOXL]$^-$ and [MoO(XH)L] (X = O, S). In addition, ^{33}S ($I = {}^3/_2$) hyperfine matrices were derived for the thio ligand in [MoOSL]$^-$ and for the sulfur atom of the mercapto ligand SH in [MoO(SH)L] for comparison with the ^{33}S coupling observed in a number of XnO ESR signals. Detailed comparisons confirm [$Mo^{V}O$(SH)] and [$Mo^{V}O$(OH)] centers as the source of the Rapid Type 1 and Slow signals of XnO and provide compelling evidence that [$Mo^{V}OS$] is responsible for the Very Rapid signal. Some preliminary aspects of this work have been reported previously.[17]

Experimental Section

Materials. $Bu^n_4NBH_4$ (Aldrich) and $Bu^n_4NBF_4$ (Southwestern Analytical) were dried under vacuum at 100 and 120 °C, respectively. Bu^n_4NSH was obtained from Fluka Chemicals. MoO_3 substituted with ^{95}Mo (96.43 atom %) or ^{98}Mo (98.75 atom %) was obtained from Oak Ridge National Laboratories and converted to anhydrous Na_2MoO_4.[22] Elemental sulfur substituted with ^{33}S (99.25 atom %) was purchased from Alfred Hempel GMBH, Dusseldorf.

Xanthine Oxidase (XnO). The enzyme used in the present work was isolated from fresh cows' milk by using a procedure developed by Hanson.[23] The general strategy was release of XnO from the milk fat globule membrane by the nonionic detergent Triton X-100, followed by removal of lipids and caseins and protein fractionation by successive extraction, precipitation, and chromatographic steps. The final steps involved cation exchange chromatography (Whatman CM-52) in KMes buffer (10 mM; pH 6.0; 0.1 mM EDTA) using a 0.1 M KCl gradient as eluent. The enzyme was desalted (Sephadex G25) into bicine buffer (50 mM; pH 8.2), carefully degassed, and stored anaerobically as frozen beads at 77 K.

Yields of about 500 mg of enzyme were obtained routinely from 45 L of milk, although yields up to 70% higher are achievable late in the lactation period when milk fat content is higher. The spectroscopic ratios PFR (A_{280}/A_{450}) and Fl/Fe (A_{450}/A_{550}) observed were 5.1 (σ 0.2) and 3.0 (σ 0.2). Values of 5.0 and 3.0 are characteristic of highly purified preparations with Fe_2S_2 and FAD centers intact.[24,25] The standard activity ratio AFR ($\Delta A_{295}/A_{450}$) measuring the rate of xanthine conversion has a value of 210 for purely functional enzyme.[26,27] Values of 125 (σ 20) were observed in the present work, indicating about 60% functionality. Molybdenum assays using a Varian GTA-95 graphite tube atomizer revealed the Mo content to be 0.71 (σ 0.04) g atoms/mol of FAD.

Polyacrylamide gel electrophoresis under nondissociating conditions revealed a single component suggestive of homogeneous preparations. Dissociating conditions (PAGE-SDS) revealed a band at 145 (±5) kDa consistent with the molar mass of 283–303 kDa estimated previously.[24,28-30] Minor bands (~5% of total stained protein) were present at 123, 89, and 58 kDa. The pattern is characteristic of limited proteolysis,[28-31] indicating that a low proportion of the intact molecules have cleaved protein backbones.

Treatment of active enzyme with cyanide converted it to the desulfo form, which itself could be reactivated routinely to 65% of its original activity via anaerobic addition of sulfide to dithionite-reduced enzyme in the presence of methylviologen.[33]

Enzyme enriched with ^{95}Mo was isolated from milk obtained from cows injected with $Na_2{}^{95}MoO_4$. The procedure was adapted from Bray.[34] The molybdate (337 mg) in deionized water (10 cm^3) was injected into the jugular vein of each cow with an equivalent booster after 36 h. Milk was collected over 72 h (six milkings). Isolated enzyme exhibited properties similar to those described above and, in particular, contained 0.75 g atoms Mo/mol of FAD. Computer simulation of EPR signals (vide infra) indicated ^{95}Mo content to be about 80 atom %.

Enzyme enriched in ^{2}H was obtained by freeze-drying frozen beads in an all-glass apparatus to a background pressure of $<10^{-3}$ mmHg, followed by dissolution in ^2H_2O (99.9 atom % ^{2}H). After removal of some denatured protein, the characterization parameters were similar to those of the original sample except that about 20% of the original activity was lost, presumably due to formation of desulfo and/or demolybdo enzyme.

Molybdenum(V) Analogue Compounds. All manipulations of molybdenum species in solution were performed under purified argon or dinitrogen gas by using standard Schlenk and gas-tight syringe techniques. Solvents were dried and fractionally distilled under inert atmosphere. In particular, EtOH was predried over CaO and distilled twice from Mg(OEt)$_2$; THF was predried over Na metal and distilled from Na met-

(14) Farchione, F.; Hanson, G. R.; Rodrigues, C. G.; Bailey, T. D.; Bagchi, R. N.; Bond, A. M.; Pilbrow, J. P.; Wedd, A. G. *J. Am. Chem. Soc.* **1986**, *108*, 831–832.
(15) Hinshaw, C. J.; Spence, J. T. *Inorg. Chim. Acta* **1986**, *125*, L17–18.
(16) Dowerah, D.; Spence, J. T.; Singh, R.; Wedd, A. G.; Wilson, G. L.; Farchione, F.; Enemark, J. H.; Kristofzski, J.; Bruck, M. *J. Am. Chem. Soc.* **1987**, *109*, 5655–5665.
(17) (a) Wilson, G. L.; Kony, M.; Tiekink, E. R. T.; Pilbrow, J. R.; Spence, J. T.; Wedd, A. G. *J. Am. Chem. Soc.* **1988**, *110*, 6923–6925. (b) Wedd, A. G.; Spence, J. T. *Pure Appl. Chem.* **1990**, *62*, 1055–1058.
(18) Singh, R.; Spence, J. T.; George, G. N.; Cramer, S. P. *Inorg. Chem.* **1989**, *28*, 8–10.
(19) Hinshaw, C. J.; Gang, P.; Singh, R.; Spence, J. T.; Enemark, J. H.; Bruck, M.; Kristofzski, J.; Merbs, S. L.; Ortega, R. B.; Wexler, P. A. *Inorg. Chem.* **1989**, *28*, 4483–4491.
(20) Gutteridge, S.; Tanner, S. J.; Bray, R. C. *Biochem. J.* **1978**, *175*, 887–897.
(21) (a) Hanson, G. R.; Wilson, G. L.; Bailey, T. D.; Pilbrow, J. R.; Wedd, A. G. *J. Am. Chem. Soc.* **1987**, *109*, 2609–2616 and references therein. (b) Froncisz, W.; Aisen, W. *Biochem. Biophys. Acta* **1982**, *700*, 55–58.
(22) Hanson, G. R.; Brunette, A. A.; McDonell, A. C.; Murray, K. S.; Wedd, A. G. *J. Am. Chem. Soc.* **1981**, *103*, 1953–1959.
(23) Hanson, G. R. Ph.D. Thesis, La Trobe University, 1984.
(24) Bray, R. C. In *The Enzymes*, 3rd ed.; Boyer, P. D., Ed.; Academic Press: New York, 1975; Vol. 12, (a) pp 299–419; (b) pp 306–310.
(25) Rajagopalan, K. V.; Handler, P. *J. Biol. Chem.* **1964**, *239*, 1509–1514.
(26) Massey, V.; Komai, H.; Palmer, G.; Ellion, G. L. *J. Biol. Chem.* **1970**, *245*, 2837–2844.
(27) Edmondson, D.; Massey, V.; Palmer, G.; Beacham, L. M., III.; Ellion, G. B. *J. Biol. Chem.* **1972**, *247*, 1597–1604.
(28) Coughlan, M. P. In ref 3, pp 119–185.
(29) Waud, W. R.; Brady, F. P.; Wiley, R. D.; Rajagopalan, K. V. *Arch. Biochem. Biophys.* **1975**, *169*, 695–701.
(30) Nagler, L. G.; Vartanyan, L. S. *Biochim. Biophys. Acta* **1976**, *427*, 78–90.
(31) Waud, W. R.; Rajagopalan, K. V. *Arch. Biochem. Biophys.* **1976**, *172*, 365–379.
(32) Massey, V.; Edmondson, D. *J. Biol. Chem.* **1970**, *245*, 6595–6598.
(33) Wahl, R. C.; Rajagopalan, K. V. *J. Biol. Chem.* **1982**, *257*, 1354–1359.
(34) Bray, R. C.; Meriwether, L. S. *Nature* **1966**, *212*, 467–469.

Table I. EPR Parameters for Xanthine Oxidase[a]

signal[b]	g				A(^{95}Mo)					A(^{1}H)				ref
	x	*y*	*z*	av	*x*	*y*	*z*	av	α_{xy}, α_{xz}[c]	*x*	*y*	*z*	av	
Rapid Type 1														
1-methylxanthine	1.9646	1.9691	1.9886	1.9741						12.8	12.8	12.0	12.5	51, 53
										1.8	2.8	3.7	2.8	
			d		24.8	24.8	61.7	37.1	0, 20			*d*		this work
formamide	1.9666	1.9710	1.9901	1.9759	25.7	24.7	61.4	37.4	0, 18	12.1	11.6	11.3	11.7	13
Rapid Type 2														
borate	1.9630	1.9695	1.9911	1.9745						15.1	14.0	13.0	14.0	38
										12.8	9.8	9.3	10.6	
	1.9617	1.9681	1.9897	1.9732	24.8	24.7	60.4	36.6	0, 20			*d*		this work
Very Rapid														
xanthine	1.9494	1.9550	2.0252	1.9765	19.1	18.2	44.4	27.2	8, 36					13
2-oxo-6-methylpurine	1.9446	1.9518	2.0229	1.9731	21.2	20.2	42.2	29.5	7, 42					13
alloxanthine	1.9442	1.9593	2.0279	1.9771										74
Slow														
aquo	1.9551	1.9671	1.9719	1.9647						14.2	15.2	15.3	14.9	20
										1.5	1.5	1.5	1.5	
	1.9542	1.9655	1.9706	1.9634	27.1	26.2	65.4	39.6	0, 33	14.2	14.8	14.9	14.6	this work
										2.1	1.5	1.3	1.6	

[a] Units: hyperfine couplings (10^{-4} cm^{-1}), angles (deg). [b] Substrate used to generate the signal is indicated. [c] α_{xy} is the angle of rotation about the *z* axis; α_{xz} is that about the new *y* axis. [d] Parameters determined in this work at S- and X-band frequencies are within experimental error of those previously estimated (see cited references).

al/Ph_2CO and finally from $LiAlH_4$ just prior to use; MeCN was predried over CaH_2 and distilled from P_2O_5.

Synthesis of LH_2 has been described previously,[16] while α-$(Bu^n_4N)_4[Mo_8O_{26}]$ substituted with ^{98}Mo or ^{95}Mo was synthesised via the method of ref 35. The latter was converted into [$^{98}MoO_2L$] and [$^{95}MoO_2L$] via the following procedure:[16] α-$(Bu^n_4N)_4[Mo_8O_{26}]$ (103 mg, 0.381 mmol of Mo) was added to MeOH (4.5 cm^3) and dissolution effected by gentle heating. After cooling to 0 °C, LH_2 (119 mg, 0.389 mmol) in CH_2Cl_2 (0.7 cm^3) was added to the clear solution. The orange precipitate which formed over 0.5 h at 0 °C was filtered, washed with cold MeOH (2 × 2 cm^3), and dried under vacuum (yield 120 mg, 79%).

EPR Samples. For XnO, and 1-methylxanthine Rapid Type 1, borate Rapid Type 2, and aquo Slow signals were generated by literature methods.[36-39]

cis-[^{95}MoO(OH)L] was generated in solution at −42 °C by reductive electrolysis at a Pt spade electrode of [$^{95}MoO_2L$] (10 mM) in THF (0.2 M $Bu^n_4NBF_4$) containing 1.5 M H_2O. The electrolysis cell was contained within an EPR sample tube of 4-mm internal diameter.[16] A potential of −1.7 V versus the ferrocinium/ferrocene couple was employed, about 0.1 V more negative than the peak cathodic current observed under the conditions. Electrolysis for about 1.5 h produced optimum EPR signal strength. The yellow-orange solution was transferred via cannula to another EPR sample tube for further examination and immediately frozen at −196 °C for storage.

[$^{95}MoO_2L$]$^-$ was prepared by bulk reductive electrolysis at a Pt electrode at 23 °C of [$^{95}MoO_2L$] (2 mM) in MeCN (0.2 M $Bu^n_4NBF_4$).[16] The potential employed was −1.5 V vs Fc^+/Fc. The yellow-brown solution was transferred via cannula to an EPR sample tube and stored frozen.

[^{95}MoOSL]$^-$ was prepared from reaction of solid [$^{95}MoO_2L$] with Bu^n_4NSH (100 mM in 1:10 MeCN/THF) to a final concentration of 5 mM in Mo, i.e., Mo:S = 1:20. The initial frozen EPR spectrum contains signals due to both [$^{95}MoO_2L$]$^-$ and [^{95}MoOSL]$^-$. Incubation at room temperature leads to [^{95}MoOSL]$^-$ only, and the signal does not lose intensity upon standing at room temperature.

cis-[^{95}MoO(SH)L] was prepared in an EPR sample tube from the solutions of [^{95}MoOSL]$^-$ described above. A degassed solution of CF_3CO_2H (200 mM in THF) was layered onto the Mo solution frozen in liquid nitrogen and itself frozen. The Mo:S:CF_3CO_2H ratios were 1:20:40–100. The higher proportion of CF_3CO_2H usually provides a stronger EPR signal. The two layers were thawed at ca. −95 °C and shaken vigorously to produce a blue solution. The samples were maintained at temperatures below −78 °C and stored frozen.

cis-[^{95}MoO(S^2H)L] was prepared similarly with Mo:S:CF_3CO_2H = 1:20:40, but the CF_3CO_2H solution was also 1 M in ^2H_2O.

For preparation of ^{33}S-substituted samples, $Bu^n_4NBH_4$ (25.7 mg, 100 mmol) in EtOH (2.1 cm^3) was added to elemental sulfur (2.9 mg, 87 mmol). Stirring produced a bright yellow solution and a steady evolution of gas. After 1.5 h, volatiles were removed under vacuum and the residue was dried at 30 °C at 0.05 mmHg pressure to produce an orange-brown film. Addition of MeCN (0.2 cm^3) followed by THF (1.8 cm^3) produced a green solution which was added to [$^{98}MoO_2L$] (4.7 mg, 11 mmol). The initial brown-green solution rapidly turned yellow. The subsequent generation and handling of solutions of [^{98}MoO(^{33}S)L]$^-$ and [^{98}MoO(^{33}SH)L] followed the procedures described above.

EPR Measurements. Varian E-9 and E-12 spectrometers operating at X-band (ca. 9.1 GHz) and using E23 cavities were employed. The low-frequency measurements were carried out by using a home-built 1–4-GHz tunable reference arm bridge attached to the E-12 spectrometer. Home-built loop gap resonators[21] tuned at 3.6 and 2.4 GHz were manufactured from Macor ceramic and subsequently silver plated. Frequencies were measured with an EIP 548-A frequency counter. Magnetic field calibration was obtained via the proton resonance of water. Spectra were recorded on an LSI 11/23 microcomputer coupled to a VAX 11/780 computer. Computer simulations employed the methods of ref 21a.

Results

Xanthine Oxidase. The enzyme used in the present work was isolated in the absence of proteolytic reagents to minimize cleavage of the protein backbone.[28-31] It was about 60% functional with Mo:FAD = 0.71. Consequently, the samples consist of 60% active ($Mo^{VI}OS$), 11% inactive desulfo ($Mo^{VI}O_2$), and 29% inactive demolybdo centers. The latter probably retain a form of the pterin cofactor.[40,41]

The Mo content appears to be a factor of local nutritional conditions.[24b,40] The content did not change significantly as a function of either the dairy employed or the isolation protocol. The methods of Rajagopalan,[29] Ball,[42] and Massey[43] provided results similar to those of the present procedure. The latter two methods use proteolytic reagents to release the enzyme and lead to extensive peptide cleavage,[28-31] which however, does not appear to affect catalytic and spectral properties. Folate affinity chromatography[40,44] is capable of separating active and desulfo centers but does not significantly improve the Mo content of the present

(35) Filowitz, M.; Ho, R. K. C.; Klemperer, W. G.; Shum, W. *Inorg. Chem.* **1979**, *18*, 93–103.
(36) Gutteridge, S.; Malthouse, J. P. G.; Bray, R. C. *J. Inorg. Biochem.* **1979**, *11*, 355–360.
(37) Malthouse, J. P. G.; Williams, J. W.; Bray, R. C. *Biochem. J.* **1981**, *197*, 421–425.
(38) Malthouse, J. P. G.; Gutteridge, S.; Bray, R. C. *Biochem. J.* **1980**, *185*, 767–770.
(39) Lowe, D. J.; Barber, M. J.; Pawlik, R. T.; Bray, R. C. *Biochem. J.* **1976**, *155*, 81–85.
(40) Ventom, A. M.; Deistung, J.; Bray, R. C. *Biochem. J.* **1988**, *255*, 949–956.
(41) Johnson, J. L.; London, R. E.; Rajagopalan, K. V. *Proc. Natl. Acad. Sci. U.S.A.* **1989**, *86*, 6493–6497.
(42) Ball, E. G. *J. Biol. Chem.* **1939**, *128*, 51–67.
(43) Massey, V.; Brumby, P. E.; Komai, H.; Palmer, G. *J. Biol. Chem.* **1969**, *244*, 1682–1691.
(44) Nishino, J.; Nishino, K.; Tsushima, K. *FEBS Lett.* **1981**, *131*, 369–372.

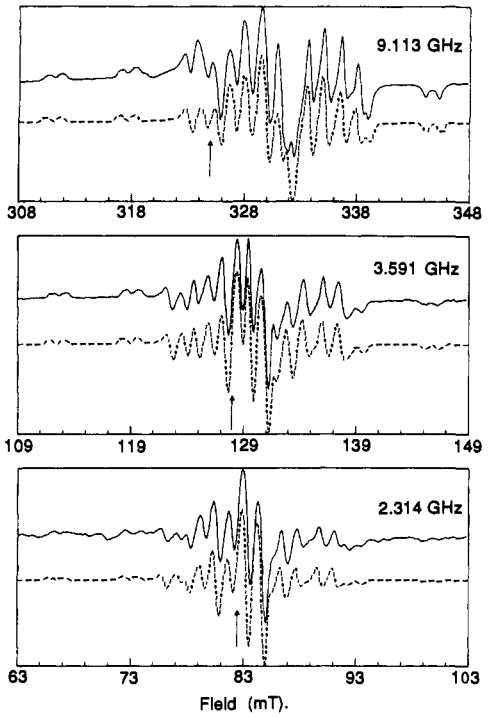

Figure 1. Experimental (solid line) and simulated (dashed line) spectra of the 1-methylxanthine Rapid Type 1 Mo^V EPR signal of XnO (^{95}Mo, 80 atom %). The arrow indicates the expected resonance position of contaminating FADH radical from the flavin site.

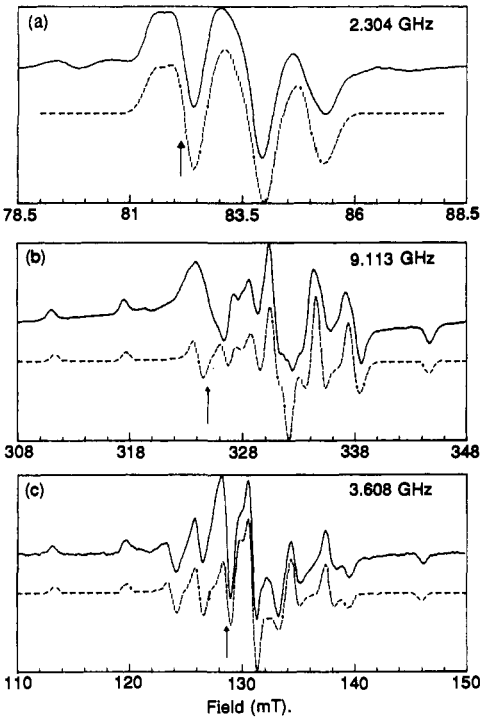

Figure 2. Experimental and simulated spectra of the borate Rapid Type 2 Mo^V EPR signal of XnO: (a) native enzyme in ^1H_2O, (b) and (c) ^{95}Mo-enriched (80 atom %) in ^2H_2O. The arrow indicates the expected resonance position of contaminating FADH radical.

preparations as the demolybdo centers are distributed statistically among dimeric molecules. Selective denaturation of demolybdo subunits with salicylate does increase the Mo content,[40,45] but the yield is low.

The reactivation of desulfo XnO can be achieved by sulfide addition to dithionite-reduced enzyme in the presence of methylviologen.[33] In the present work, *both* methylviologen (apparently used originally[33] as an "indicator of anaerobicity") and dithionite were essential for reactivation. In the presence of excess sulfide, desulfo XnO treated with dithionite only (20–1500 equiv) or with electrochemically reduced methylviologen only (50–850 equiv) failed to achieve appreciable reactivation after 2 h of incubation. Addition of the missing component induced rapid reactivation. Reports[46,47] disputing the original observations may have omitted the methylviologen from the procedure. Watt[48] has reported that dithionite reduction of $3e^-$-reduced nitrogenase is very slow unless methylviologen is present.

Enzyme EPR Signals. The present work concentrates on estimation of the ^{95}Mo hyperfine parameters for the Rapid Types 1 and 2 and Slow signals of XnO (Table I) derived from experimental spectra generated in both ^1H_2O and ^2H_2O at three different frequencies. Representative spectra are given in Figures 1–3.

The expectation of improved resolution of the various hyperfine couplings seen in XnO spectra was not realized in the present work. The XnO S-band (2–4 GHz) spectra observed here have line widths comparable to the X-band signals, indicating that the g and A strain contributions to the X-band line widths are unexpectedly small. It would appear that the globular protein structure in this large enzyme buffers the Mo center against microscopic variations in coordination geometry induced by freezing to the glassy state. Certainly, simulations of good quality (Figures 1–3) were obtained without use of the g and A strain parameters C_1 and C_2 in the line width estimates.[21a,49] Such effects are seen, however, in increased line widths at the higher Q-band frequencies (e.g., refs 50 and 51). The expected improved resolution at the

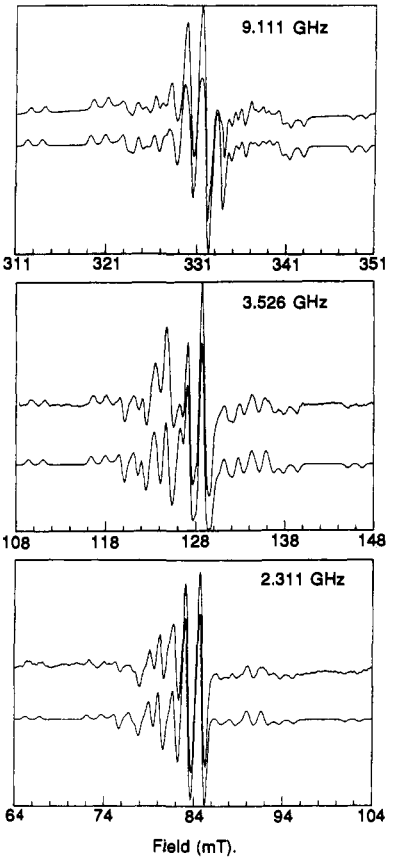

Figure 3. Experimental and simulated spectra of the aquo Slow Mo^V EPR signal of XnO (^{95}Mo, 80 atom %).

(45) Hart, L. I.; McGartoll, M. A.; Chapman, H. R.; Bray, R. C. *Biochem. J.* **1970**, *116*, 851–864.
(46) Hille, T.; Massey, V. In ref 2, pp 443–518.
(47) Venton, A.; Bray, R. C. In *Flavins and Flavoproteins*, Bray, R. C., Engel, P. C., Mayhew, S. G., Eds.; Walter de Gruyter: Berlin, 1984, 695–698.
(48) Watt, G. *Biochemistry* **1986**, *25*, 5196–5202.
(49) Pilbrow, J. R. *J. Magn. Reson.* **1984**, *58*, 186–203.

Table II. EPR Parameters for *cis*-Molybdenum(V) Compounds[a,b]

	g				A(^{95}Mo)					A(^{1}H)			
species	*x*	*y*	*z*	av	*x*	*y*	*z*	av	α_{xz}[c]	*x*	*y*	*z*	av
$[MoO_2L]^-$	1.9868	1.9158	1.8106	1.9044	27.08 (2)	31.20 (2)	68.8 (2)	42.4 (2)	0				
[MoO(OH)L]	1.9438	1.9470	1.9805	1.9571	24.5 (1)	29.0 (1)	64.0 (1)	39.2 (2)	26 (1)	20.0 (1)	10.5 (1)	13.9 (1)	14
[MoO(SH)L]	1.9523	1.9598	2.0155	1.9759	23.3 (1)	23.1 (1)	51.1 (1)	34.1 (2)	16 (1)	11.4 (1)	10.1 (1)	8.5 (1)	10
$[MoOSL]^-$	1.8885	1.9336	2.0165	1.9462	22.63 (1)	23.5 (1)	53.5 (3)	33.2 (3)	36 (1)				

[a] Units: coupling constants (10^{-4} cm^{-1}), angles (deg). [b] For *g* values, errors are considered to be ±0.0004. For hyperfine coupling, errors in fitting are indicated in parentheses. [c] α_{xz} is the angle of rotation about the *y* axis.

Table III. ^{33}S Hyperfine Parameters[a]

center[b]	*x*	*y*	*z*	av	α_{xy}[c]	α_{yz}[c]	ref
Very Rapid							
2-oxo-6-methylpurine	5.4	27.4	2.8	11.9	30	10	13
xanthine	6.4	25.6	2.8	11.5	40	10	13,53
$[MoOSL]^-$	7.2 (1)	21.5 (1)	3.8 (1)	10.8 (2)	0	0	this work
[MoO(SH)L]	2.2 (1)	0.8 (1)	1.1 (1)	1.4 (2)	0	0	this work
Rapid Type 1							
1-methylxanthine	3.3	3.3	3.2	3.3			53
Rapid Type 2							
borate	3.2	2.0	3.4	2.9			53
alloxanthine	6.4	28.4	2.8	12.6	50	10	74

[a] Units: coupling constants (10^{-4} cm^{-1}), angles (deg). [b] Substrate used to generate the enzyme signal is indicated. [c] α_{xy} is the angle of rotation about the *z* axis; α_{yz} is that about the new *x* axis.

lower frequencies is, however, observed for the model compounds, which exhibit larger line widths than those typically observed in the enzyme signals.

Parameter estimates for **g** and A(^{1}H) were obtained from the $I = 0$ resonances of samples at natural abundance in Mo dissolved in ^2H_2O and ^1H_2O, respectively. The effects upon the spectra of noncoincidence of the diagonal frames of reference of the **g** and A(^{95}Mo) matrices are minimized at the lower frequencies.[21,69] This assists in the simulation of spectra from the ^{95}Mo-enriched samples for these low-symmetry enzyme sites.

Attention was initially focused on the ^{2}H spectrum at 2.3 GHz for preliminary estimation of A(^{95}Mo). These estimates were then refined at the two higher frequencies until a parameter set was obtained that adequately reproduced the experimental spectra at all frequencies (Table I, Figures 1-3). A ^{95}Mo ($I = {}^5/_2$):^{98}Mo ($I = 0$) atom ratio of 80:20 was assumed in the simulations. A(^{2}H) was assumed to be related to A(^{1}H) by dividing the individual components by 6.51, the ratio of the gyromagnetic ratios.

The principal values of **g** and A(^{1}H) matrices have been estimated previously[13,52] from experiments at X-band (9 GHz) and Q-band (35 GHz) frequencies (Table I). That these values or very similar ones (Table I) simulate the relevant features of the spectra observed at 3.6 and 2.3 GHz (S-band) in the present work provides strong confirmation of those estimates.

The 1-methylxanthine Rapid Type 1 signal (Figure 1) features coupling to two inequivalent protons (Table I).[51,53] The **g** and A(^{95}Mo) matrices are close to axial with their diagonal frames of reference misaligned by about 20° in the *xz* plane. The largest component of A(^{95}Mo), A_z, is associated with the extreme low field *g* value, g_z.

The borate Rapid Type 2 signal also exhibits coupling to two protons.[38] The "triplet" appearance of the $I = 0$ resonance at 2.3 GHz (Figure 2a) confirms that coupling to each proton is nearly isotropic and of similar magnitude (Table I). The **g** matrices of the Rapid Type 1 and 2 signals are similar,[38] and generation of the ^{2}H signal using ^{95}Mo-enriched enzyme shows that the similarity extends to the A(^{95}Mo) matrix (Table I; Figure 2b and c).

The aquo Slow signal features coupling to two inequivalent protons, but the coupling constants are respectively larger and smaller than those seen in the Rapid Type 1 signal.[20,54,55] The

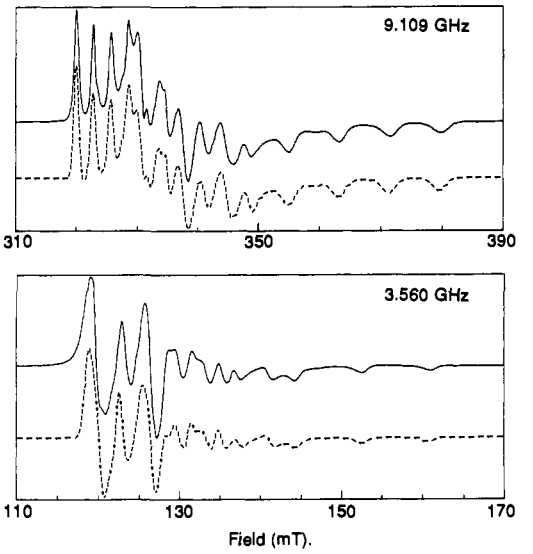

Figure 4. Experimental and simulated EPR spectra of $[MoO_2L]^-$ (^{95}Mo, 96.43 atom %).

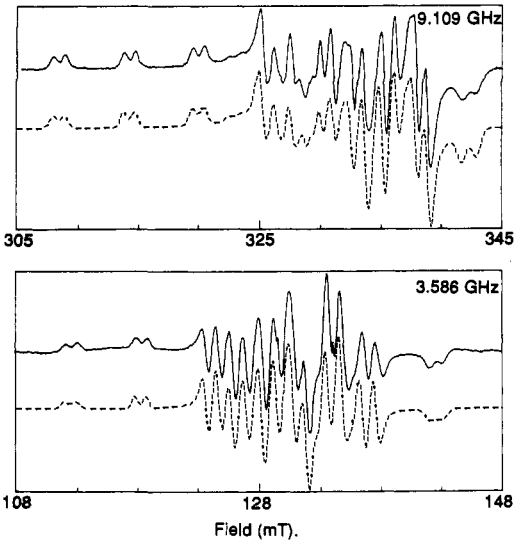

Figure 5. Experimental and simulated EPR spectra of [MoO(SH)L]$^-$ (^{95}Mo, 96.43 atom %).

(50) Bray, R. C.; Vanngard, T. *Biochem. J.* **1969**, *114*, 725-734.
(51) Gutteridge, S.; Tanner, S. J.; Bray, R. C. *Biochem. J.* **1978**, *175*, 869-878.
(52) Bray, R. C. In *Biological Magnetic Resonance*; Berliner, L. J., Reuben, J., Eds.; Plenum Press: New York, 1980; Vol. 2, pp 45-84.
(53) Malthouse, J. P. G.; George, G. N.; Lowe, D. J.; Bray, R. C. *Biochem. J.* **1981**, *199*, 629-637.

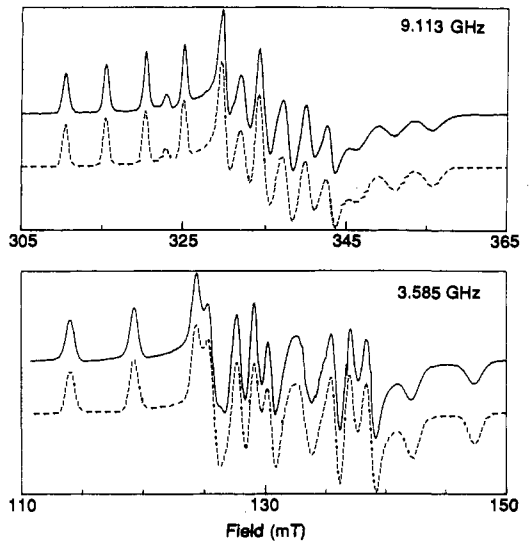

Figure 6. Experimental and simulated EPR spectra of $[MoOSL]^-$ (^{95}Mo, 96.43 atom %).

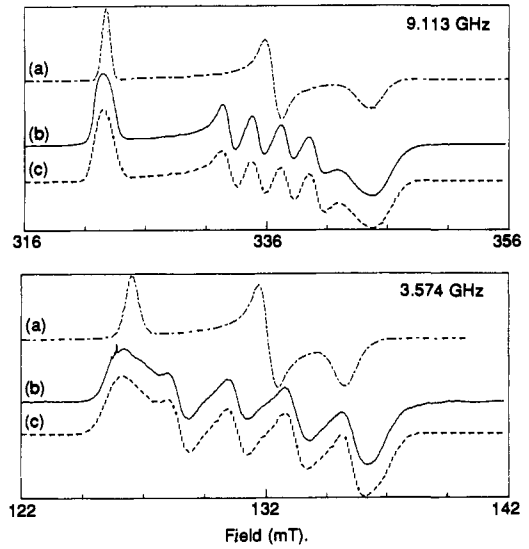

Figure 7. EPR spectra of $[MoOSL]^-$ (^{98}Mo, 98.72 atom %): (a) S isotopes at natural abundance ($I = 0$, 99.22 atom %), (b) ^{33}S ($I = {}^3/_2$; 99.25 atom %), (c) simulation of (b).

magnitude of the coupling in A(^{95}Mo) is similar in both signals (Table I) with the misalignment of g and A(^{95}Mo) frames of reference larger (33°) for the Slow signal.

The Rapid Types 1 and 2 signals, as well as the glycolaldehyde Inhibited signal,[37] were also generated from samples enriched with ^{33}S (59.15 atom %; $I = {}^3/_2$). Coupling was observed in each signal, but disappointingly, resolution was not enhanced at S-band frequencies. However, in each case, the low-frequency spectra could be simulated by using the estimates of A(^{33}S) obtained previously (Table III), substantiating those estimates.

EPR Signals of Molybdenum(V) Analogue Compounds. The multifrequency spectra were simulated by using an approach similar to that used above for the enzyme signals. In particular, the components of g, A(^{1}H), and A(^{95}Mo) for $[MoOXL]^-$ and *cis*-[MoO(XH)L] (X = O, S) were derived progressively from (^{98}Mo, ^{2}H)-, (^{98}Mo, ^{1}H)-, (^{95}Mo, ^{2}H)-, and (^{95}Mo, ^{1}H)-substituted materials examined at two different frequencies at least. Estimation of A(^{33}S) employed (^{98}Mo, ^{33}S) substitution. Selected spectra are given in Figures 4–7 and derived parameters listed in Tables II and III. The importance of using ^{95}Mo-enriched materials for accurate estimation of A(^{95}Mo) has been empha-

(54) Bray, R. C.; Gutteridge, S. *Biochemistry* **1982**, *21*, 5992–5999.
(55) Kony, M. Ph.D. Thesis, La Trobe University, 1988.

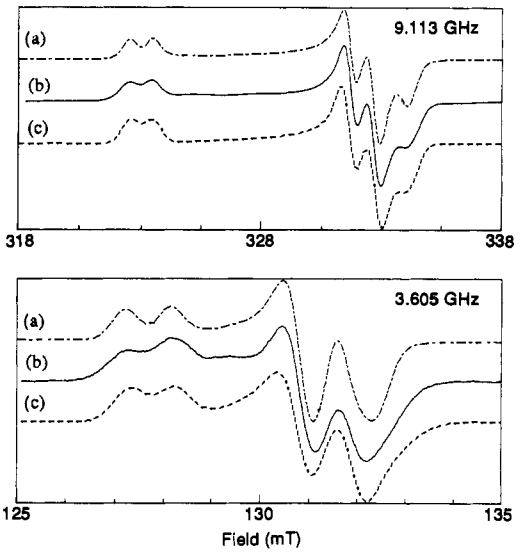

Figure 8. EPR spectra of [MoO(SH)L] (^{98}Mo, 98.75 atom %): (a) S isotopes at natural abundance ($I = 0$, 99.22 atom %), (b) ^{33}S ($I = {}^3/_2$; 99.25 atom %), (c) simulation of (b).

sized:[13] uncertainties result from neglect of quadrupolar coupling in the ^{97}Mo-containing species in naturally occurring molybdenum.

The simulations indicated (Table II; Figures 4–6) that the components of g and A(^{95}Mo) are misaligned significantly (15–36°) in one plane for [MoO(XH)L] and $[MoOSL]^-$, but not for $[MoO_2L]^-$. On the other hand, satisfactory simulation of the spectra of ^{33}S-enriched $[MoOSL]^-$ and [MoO(SH)L] at the resolution attained (Figures 7 and 8) was possible assuming that the components of g and A(^{33}S) were coincident and that coupling to a single sulfur atom was present.

The components of A(^{95}Mo) reported in Table II for $[MoOSL]^-$ differ from those originally reported.[16] As pointed out previously,[13,17] both parameter sets fit the X-band spectrum adequately. Those given in Table II are now confirmed as they satisfactorily fit the observed spectra at three different frequencies. The original values do not. A similar situation applies to the original[11,34] and revised[13] parameter sets reported for the Very Rapid signals of XnO.

Discussion

^{95}Mo Coupling in XnO Signals. This work defines A(^{95}Mo) for the Rapid Type 1, Rapid Type 2, and Slow signals of XnO. George and Bray[13] have recently provided those for the Very Rapid and Rapid Type 1 signals, as well as ^{97}Mo quadrupole coupling matrices. The parameters listed in Tables I and III adequately simulate spectra over frequencies from 2 to 35 GHz and can be accepted with considerable confidence. Interestingly, the Rapid Type 1 spectrum of ^{95}Mo-enriched XnO was first published over 20 years ago. That it has taken until recently to define properly the ^{95}Mo hyperfine matrix for it and related signals emphasizes the challenge of simulating EPR signals from Mo^V centers of low symmetry (monoclinic, triclinic).

The relative orientation of the components of g and A(^{95}Mo) is a coarse indicator of the symmetry at the metal site. The monoclinic symmetry (g and A(^{95}Mo) misaligned in a single plane) of the Rapid Type 1, Rapid Type 2, and Slow signals (Table I) suggests effective C_s or C_2 point symmetry for the Mo chromophore, while the triclinic nature of the Very Rapid signal indicates low point symmetry, C_i or C_1.[13]

The g matrices of the Rapid Type 1 and Rapid Type 2 signals are very similar.[38] This similarity extends to A(^{95}Mo) (Table I) and confirms the close relationship of the two centers responsible for the signals.

^{95}Mo Coupling in [MoO(OH)L] and $[MoO_2L]^-$. Quantitative structural information is not available for either of these species. However, the frozen solution EPR spectra of *cis*-[MoO(OR)L] (R = ^{2}H, $SiMe_3$) in THF virtually superimpose,[17,55] indicating similar structures. Consequently, the structure of [MoO(OH)L]

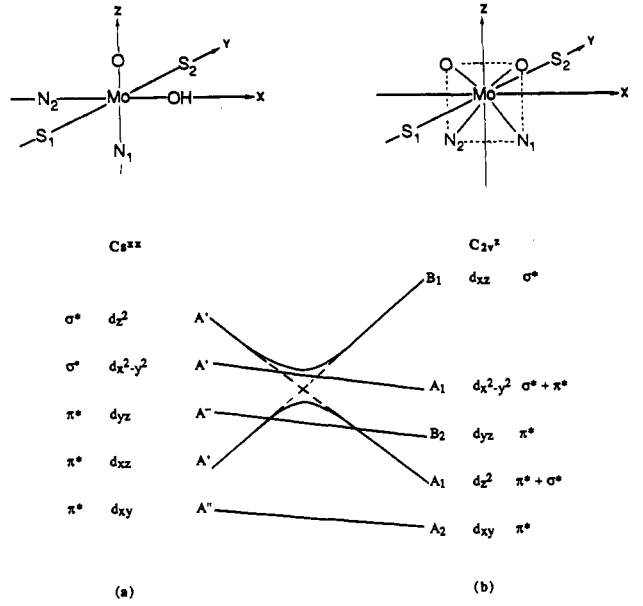

Figure 9. Correlation diagram for [MoO(OH)L] (C_s^{xz}) and $[MoO_2L]^-$ (C_{2v}^{z}).

is assumed to be close to that of *cis*-[MoO(OSiMe$_3$)L].[17] The point symmetry of $[Mo^{VI}O_2L]$ is close to C_2 symmetry,[16] and the structure of $[MoO_2L]^-$ is assumed to be similar.[56] Both of the defined structures have short MoO distances close to 1.7 Å, indicating that the multiply bonding oxo ligands dominate the ligand field. The electronic spectra of the Mo^V species feature intense absorptions ($\epsilon > 10^3$ M^{-1} cm^{-1}),[16] which have not been analyzed in detail. Certainly, ligand field bands have not been observed, and the relative energies of the d-based valence levels are unknown.

The EPR spectra of [MoO(OH)L] and $[MoO_2L]^-$ show spectacular differences.[16] The latter is the most anisotropic Mo^V spectrum known. In addition, the largest component of A(^{95}Mo) is associated with the low-field component of **g** (1.9805) in [MoO(OH)L] but with the high-field component (1.8106) in $[MoO_2L]^-$ (Table II).

The observed EPR spectrum of [^{95}MoO(OH)L] can be simulated assuming an angle of rotation of 26° about the middle **g** component. Hence, this **g** axis and the associated **A** axis are coincident. This is consistent with C_s^{xz} local symmetry (Figure 9a), which predicts that g_y and A_y(^{95}Mo) will be coaxial but that the principal axes in the *xz* plane may not be. This assignment is assumed in Table II. Similar situations have been examined previously,[57-61] and the order of the d-based valence levels is expected to be that listed in Figure 9a. In the present case, the magnetic orbital (HOMO) is expected to be of the form

$$\phi(A'') = a(d_{xy}) + b(d_{yz}) \quad (1)$$

We may attempt to gain some insight into the electronic behavior of Mo^V in both the enzyme and analogue complexes by assuming that the magnetic orbital is essentially a d_{xy} orbital by putting $a \approx 1$ and $b \approx 0$ in the theory of the *g* and *A* values.[57,58] Further, we ignore the effects of covalent bonding. The theory, correct to first order in spin–orbit coupling, leads to the following results, which may be compared with those given by McGarvey[57] for $d_{x^2-y^2}$:

$$g_z = 2.00 - \frac{8\zeta}{\Delta E_{x^2-y^2}} \quad (2)$$

$$g_x = 2.00 - \frac{2\zeta}{\Delta E_{xz}} \quad (3)$$

$$g_y = 2.00 - \frac{2\zeta}{\Delta E_{yz}} \quad (4)$$

$$A_z = P\left\{-\kappa - 4/7 - \frac{3\zeta}{7\Delta E_{yz}} - \frac{3\zeta}{7\Delta E_{xz}} - \frac{8\zeta}{\Delta E_{x^2-y^2}}\right\} \quad (5)$$

$$A_x = P\left\{-\kappa + 2/7 + \frac{3\zeta}{7\Delta E_{yz}} - \frac{2\zeta}{\Delta E_{xz}}\right\} \quad (6)$$

$$A_y = P\left\{-\kappa + 2/7 - \frac{2\zeta}{\Delta E_{yz}} + \frac{3\zeta}{7\Delta E_{xz}}\right\} \quad (7)$$

where $\Delta E_i = E_i - E_{xy}$, ζ is the spin–orbit coupling constant for Mo^V in the complex, $P = g_e g_N \beta_e \beta_N \langle r^{-3} \rangle_{4d}$, and κ is the isotropic hyperfine constant in the complex. In eqs 3–7, it is assumed that $\Delta E_{xz} = \Delta E_{yz}$, whereas they would be strictly equal only in the limit of axial symmetry.

Despite the gross approximations

$$g_x \approx g_y \qquad |A_z| > |A_x|, |A_y| \quad (8)$$

are firm predictions from eqs 2–7 given that the crystal field order of energy levels given in Figure 9a is reasonable and that $\kappa \approx 0.9$ for Mo^V.[62] The assignment of the spectrum of [MoO(OH)L] provided in Table II is made from predictions 8. A_z should be directed close to the *z* axis (MoO direction), but any symmetry mixing of d_{yz} into d_{xy} will rotate the magnetic orbital about the *y* axis, resulting in some rotation of g_z in the *xz* plane away from the *z* axis and an accompanying rotation of g_x. The interpretation is consistent with previous studies of [Mo^VO] and related species.[61-63]

The above theory and the conclusions drawn so far must be regarded as tentative.[63,66] However, the patterns of **g** and **A**(^{95}Mo) and the values of the misalignment angle α_{xz} reported for [MoO(OH)L] and for the enzyme signals (Tables I and II) are consistent with the general indications of the above model. Values of α_{xy} for the enzyme signals are all zero or sufficiently small that the existing level of theory can offer no definitive insight. Only $[MoO_2L]^-$ exhibits a different general behavior.

We now turn to the exceptional case of $[MoO_2L]^-$. While the point symmetry is assumed to be C_2, the observed ESR spectrum

(56) While *cis*-MO_2 species are numerous for the d^0 configuration, only two structurally characterized examples of six-coordinate *cis*-MO_2 complexes are known for d^n ($n > 0$). They are both d^2 species, $[ReO_2(py)_2(bpy)]$: (a) Blackburn, R. L.; Jones, L. M.; Ram, M. S.; Sabat, M.; Hupp, J. T. *Inorg. Chem.* **1990**, *29*, 1791–1792. (b) Ram, M. S.; Hupp, J. T. *Inorg. Chem.* **1991**, *30*, 130–133. $[OsO_2(CH_3CO_2)_3]^+$: Behling, T.; Caparelli, M. V.; Skapski, A. C.; Wilkinson, G. *Polyhedron* **1982**, *1*, 840–841.

(57) McGarvey, B. R. In *Transition Metal Chemistry*; Carlin, R. L., Ed.; Dekker: New York, 1966; Vol. 3, pp 89–201.

(58) Hitchman, M. A.; Belford, R. L. *Inorg. Chem.* **1969**, *8*, 958–965.

(59) Garner, C. D.; Lambert, P.; Mabbs, F. E.; King, T. J. *J. Chem. Soc., Dalton Trans.* **1977**, 1191–1201.

(60) Scullane, M. I.; Taylor, R. D.; Minelli, M.; Spence, J. T.; Yamanouchi, K.; Enemark, J. H.; Chasteen, N. D. *Inorg. Chem.* **1979**, *18*, 3213–3219.

(61) Young, C. G.; Enemark, J. H.; Collison, D.; Mabbs, F. E. *Inorg. Chem.* **1987**, *26*, 2925–2927.

(62) DeArmond, K.; Garett, B. B.; Gutowsky, H. S. *J. Chem. Phys.* **1965**, *42*, 1019–1025.

(63) One of us (J.R.P.) has carried out more detailed calculations for C_s^{xz} symmetry which suggest that the g_z and g_x axes are more likely to be rotated about *y* than are A_z and A_x. This is consistent with earlier results[64,65] for low-spin $3d^7$ and $3d^9$. It comes about because the *g* shifts from the free electron value are determined by spin–orbit coupling to excited orbitals, which are themselves rotated by the low-symmetry ligand field. While *g* shifts appear directly in expressions for principal *A* values in the orthorhombic limit, they play a less important role than do κ and the $^2/_7$ and $^4/_7$ terms. In short, hyperfine constants are expected to be determined primarily by the dominant orbital in the ground state rather than by spin–orbit mixing and, therefore, to have principal directions related fairly obviously to the positions of coordinating ligands.

(64) Pilbrow, J. R.; Winfield, M. E. *Mol. Phys.* **1973**, *25*, 1073–1078.

(65) Belford, R. L.; Harrowfield, B. V.; Pilbrow, J. R. *J. Magn. Reson.* **1977**, *28*, 433–439.

(66) (a) An alternative explanation for $g_z < g_x$, g_y could be derived by adapting for d^1 the theory developed by Bleaney and O'Brien[67b] for low-spin d^5 ions. (b) Bleaney, B.; O'Brien, M. C. M. *Proc. Phys. Soc., London, Sect. B* **1956**, *69*, 1216–1230.

of $[^{95}MoO_2L]^-$ (Figure 4, Table II) can be simulated assuming C_{2v} local symmetry (Figure 9b); i.e., all components of **g** and **A**(^{95}Mo) are coincident with the molecular axes and $\alpha_{xz} = 0°$.

Figure 9 correlates the raising of symmetry from C_s^{xz} in [MoO(OH)L] to C_{2v}^{z} in $[MoO_2L]^-$ to assist comparisons.[67] Note that, in a simplistic sense, the roles of d_{xz} and d_{z^2} switch to become σ- and π-antibonding, respectively, in C_{2v}^{z} symmetry, although symmetry mixing of d_{z^2}, $d_{x^2-y^2}$, and d_{xz} will blur the distinction. As an initial basis for discussion, the magnetic orbital is proposed to be d_{xy}, as suggested by crystal field considerations. If such is the case, then symmetry mixing into the ground state is not a complication in this system as d_{xy} alone belongs to the A_2 representation.

The previous model, eqs 2–7, can be applied again. As before

$$|A_z| > |A_x|, |A_y| \tag{9}$$

is the firm prediction, but Table II indicates that, in contrast to [MoO(OH)L], the largest component of **A** is associated with the smallest (highest field) component of **g**. For g_z to be that smallest component, $\Delta E_{x^2-y^2}$ must be reduced considerably from the situation in [MoO(OH)L] (eq 2).

Examination of Figure 9b indicates that $d_{x^2-y^2}$ (now directed at two S atoms *only*) will be much less σ-antibonding than d_{xz} (directed at *two* oxo and two N atoms), and so the required stabilization of $d_{x^2-y^2}$ appears plausible. In addition, the nature of d_{xz} and d_{yz} provide, via eqs 3 and 4, that

$$g_x > g_y \tag{10}$$

The assignment given in Table II is based upon predictions 9 and 10.

The above analysis based upon such a simple model can be at best preliminary.[68] Single crystal data from samples of [MoO(OH)L] and $[MoO_2L]^-$ doped into a diamagnetic lattice are needed, and the matter is currently under study. However, the implication is that differences in the EPR spectra of the two systems are associated primarily with the nature of the $d_{x^2-y^2}$-based orbital. The fact that the value of g_z in $[MoO_2L]^-$ varies significantly with the nature of L[69] supports the analysis: L supplies the ligand atoms that interact most directly with $d_{x^2-y^2}$.

^{95}Mo and ^{33}S Coupling in [MoO(SH)L] and $[MoOSL]^-$. The behavior of **g** and **A**(^{95}Mo) in [MoO(SH)L] (Figure 5) is qualitatively similar to that of [MoO(OH)L]. Quantitatively, the components of **g** are larger, those of **A**(^{95}Mo) are smaller, while α_{xz} is smaller (Table II). The changes can be traced to an increase in effective ligand spin–orbit coupling constant upon substitution of SH for OH, coupled with an increased covalent contribution to the bonding. Such effects have been seen clearly in the behavior of the anions $[MoOCl_{4-x}(SPh)_x]^-$ (x = 0–4),[22] $[MOX_4]^-$ (M = Mo, W; X = Cl, SPh, SePh),[14] and other systems.[61]

The case of $[MoOSL]^-$ is interesting in that oxo and thio are both strong π-donor ligands. However, the observed EPR spectrum (Figure 6; Table II) indicates that the oxo ligand dominates the ligand field. Superficially, the spectral features appear closely related to those of [MoO(SH)L] (C_s^{xz}, Figure 9a), with **A**(^{95}Mo) being very similar in pattern and magnitude. The largest component of **A**(^{95}Mo) is associated with the largest component of **g**, contrasting with the case of $[MoO_2L]^-$. Assignment of (g_y, A_y) follows from the simulation and of (g_z, A_z) from the magnitude of the coupling constant. Further analysis, particularly regarding the low value of g_x = 1.8885, is unwise as coupling to ^{33}S reveals the magnetic orbital to be highly covalent.

Remarkably large and anisotropic coupling is seen in $[^{98}MoO^{33}SL]^-$ (Figure 7; Table III). As canvassed previously,[13,70] the isotope ^{33}S has a small gyromagnetic ratio g_N and so hyperfine coupling tends to be small in magnitude. The anisotropy of the coupling in the present compound suggests an unpaired spin density of 0.3–0.4 electrons on the S atom. Protonation of $[MoOSL]^-$ to [MoO(SH)L] results in coupling to ^{33}S which is greatly reduced in both magnitude and anisotropy (Figure 8; Table III).

^{1}H Coupling in [MoO(XH)L] (X = O, S). As can be seen from Table II, **A**(^{1}H) is significantly anisotropic for X = O but less so for X = S. The tensor components can be factorized into isotropic, A_{iso}, and anisotropic, A_{ai}, components. For X = O, A_{iso} = 14.8, A_{ax} = 5.2, A_{ay} = −4.3, and A_{az} = -0.9×10^{-4} cm^{-1}, while for X = S, A_{iso} = 10.0, A_{ax} = 1.4, A_{ay} = 0.1, and A_{az} = -1.5×10^{-4} cm^{-1}.

The coupled proton is bound to atom X, a ligand of Mo^V. Therefore, there are two likely contributions to the observed coupling:[71] (1) A direct "through space" electron nuclear dipolar interaction. This will have magnitudes $a = 52.68/r^3$ and $-a/2 = -26.34/r^3$ (10^{-4}cm^{-1}; r (Å)) parallel and perpendicular to **r**, the MoH direction. **g** is assumed to be isotropic for the purpose of the calculation. (2) An indirect dipolar coupling, (b, $-b/2$), associated with unpaired electron density on the intermediate atom X. This would have principal directions parallel and perpendicular to the direct coupling but, except for linear or orthogonal arrangements of MoXH, would not share the same principal axes.

With these assumptions, it is possible to decompose **A**(^{1}H) for [MoO(OH)L] into two axial contributions.[72] There are, in fact, two possible decompositions,[72] and the derived parameters a translate to r(MoH) ≈ 2.0–2.4 Å corresponding to MoOH angles of 79–102° (taking r(MoO) and r(OH) as 1.9 and 1.1 Å, respectively). Similar treatment of [MoO(SH)L] suggests only one physically possible solution to a giving r(MoH) ≈ 3.1 Å corresponding to an MoSH angle of 106° (taking r(MoS) and r(SH) as 2.4 and 1.4 Å, respectively).

This simple analysis provides physically reasonable bond angles and is consistent with both direct and indirect dipolar coupling being the source of anisotropy of **A**(^{1}H) in [MoO(XH)L].

Comparison of Enzyme and Analogue Compound EPR Spectra. The Nature of the Very Rapid, Rapid Type 1, and Slow Signals. This work provides strong evidence that the following chromophores are responsible for the characteristic EPR signals of XnO: Very Rapid, Mo^VOS; Rapid Type 1, $Mo^VO(SH)$; Slow, $Mo^VO(OH)$. Comparison of average ^{1}H and ^{17}O coupling constants for enzyme and analogue compounds provided initial evidence.[14-17] This is now strongly supported by ^{33}S coupling matrices and, for the higher symmetry Rapid and Slow signals, by ^{95}Mo coupling matrices.

In particular, the distinctive pattern of ^{33}S coupling constants observed in the Very Rapid signals of XnO is reproduced so convincingly by $[^{98}MoO^{33}SL]^-$ (Table III) that there can be little doubt that a $[Mo^VOS]$ chromophore is responsible. Upon protonation to [MoO(SH)L], both the magnitude and the anisotropy of the coupling collapses. Comparison with the behavior observed for the Rapid Type 1 signals (Table III) supports previous assignment[13,16] of that signal to *cis*-$[Mo^VO(SH)]$. Thus, the Very Rapid center is a conjugate base form of the Rapid center.

This simple formulation is not consistent with pH-jump studies of XnO carried out at −60 and −82 °C in cryogenic DMSO–H_2O solvent systems.[73] Further examination of this and other systems

(67) We thank a reviewer for suggestions that clarified use of Figure 9 in subsequent discussion.

(68) As Figure 9b suggests, the possibility that the magnetic orbital in $[MoO_2L]^-$ is d_z^2-based should be considered. This requires that $|A_z| < |A_{x,y}|$.[21a] The pattern of observed values in Table II does not support such a possibility.

(69) Wilson, G. L. Ph.D. Thesis, La Trobe University, 1988.

(70) Goodman, B. A.; Raynor, J. B. *Adv. Inorg. Chem. Radiochem.* **1970**, *13*, 135–162.

(71) Hall, T. P. P.; Hayes, W.; Stevenson, R. W. H.; Wilkins, J. *J. Chem. Phys.* **1963**, *38*, 1977–1984.

(72) For [MoO(OH)L], assuming all tensor components are positive (units 10^{-4} cm^{-1}):

directions	x	y	z	
tensor comp	20	10.5	13.9	
A_{ai}	5.2	−4.3	−0.9	
option 1	a	$-a/2$	$-a/2$	a = 6.3
	$-b/2$	$-b/2$	b	b = 2.2
option 2	a	$-a/2$	$-a/2$	a = 4.1
	$-b/2$	b	$-b/2$	b = −2.2

(73) Tsopanakis, A.; Tanner, S. T.; Bray, R. C. *Biochem. J.* **1978**, *175*, 879–885.

to clarify the relationship between the Very Rapid and Rapid centers is highly desirable.

Examination of A(^{95}Mo) matrices of [MoO(SH)L] and [MoO(OH)L] (Table II) with those of the Rapid Type 1 and Slow spectra (Table I) further supports assignment of those signals to *cis*-[Mo^{V}O(SH)] and *cis*-[Mo^{V}O(OH)] centers of effective C_s point symmetry. Note that the relative magnitudes of the components and angles are reproduced.

No enzyme signal with the characteristic signature of a [Mo^{V}O$_2$] center (Table II) has been observed, even in those enzymes known to feature [Mo^{VI}O$_2$] oxidized sites.[16]

Besides providing the necessary steric barriers, ligand L was designed to supply the two thiolate ligands detected by EXAFS spectroscopy.[8-10] However, the *trans*-thiolate stereochemistry is not that proposed[6] for the molybdenum cofactor ligand, which is suggested to feature a *cis*-dithiolate function bound to an unsaturated pterin. Consequently, the properties of the chromophores more dependent upon the peripheral ligands (**g** for all the signals; A(^{95}Mo) in the lower symmetry Very Rapid signal) are modeled less satisfactorily. The presence of a thio ligand in [MoOSL]$^-$ certainly leads to $g_z > g_e = 2.0023$, a feature seen in the Very Rapid signal. This property is most likely caused by mixing of excited charge transfer states associated with a Mo^{V}OS moiety into the ground magnetic state via spin–orbit coupling.[61] However, the detailed features of **g** in the enzyme signals are not reproduced by the present models (Tables I and II).

Mechanism of Correlated Electron–Proton Transfer. The identification of Mo^{V}OS as the Very Rapid center permits a more detailed comparison of the species observed in the Mo center of XnO as a function of oxidation state:

Mo ox. state	centers		technique
VI	Mo^{VI}OS		EXAFS
V	Mo^{V}OS	Mo^{V}O(SH)	ESR
IV		Mo^{IV}O(SH) ?	EXAFS

EXAFS spectroscopy detects the short multiple MoO and MoS bond distances in the resting Mo^{VI}OS form of XnO.[8] The absence of a short MoS distance in the Mo^{IV} form is consistent with the presence of a Mo–SH link. The proton involved is almost certainly that detected as the strongly coupled proton in the Rapid Type 1 signal, and its source is the C–H linkage attacked by the enzyme.[51]

[MoOSL]$^-$ is a species with intriguing properties: (i) EXAFS does not detect a short MoS linkage in the Ph_4P^+ salt.[18] (ii) A(^{95}Mo) is very similar to that of [MoO(SH)L] (Table II). (iii) A(^{33}S) is large in one direction, with the magnetic electron providing a spin density of 0.3–0.4 electrons on the thio ligand (Table III).

Such unusual properties can be rationalized if the oxo ligand dominates the ligand field forcing the magnetic orbital into the *xy* plane (c.f. Figure 9a with S replacing OH). The stronger π-donor ability of oxo relative to thio is seen in related situations.[61,77] Valence bond structures may be written for [MoOS] centers in formal molybdenum oxidation states VI, V, and IV, which each exhibit a MoO triple bond with Mo($d_{xz,yz}$)–O($p_{x,y}$) π-components (Figure 9a):

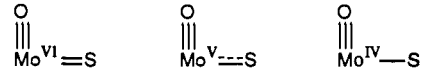

The MoS double bond in the Mo^{VI} form features a Mo(d_{xy})–S(p_y) π-interaction. The fact that a single directional component dominates the ^{33}S coupling in [Mo^{V}OSL]$^-$ indicates that the antibonding partner of the latter interaction is singly occupied, reducing the MoS bond order to 1.5 in the Mo^{V} form. Protonation collapses the coupling, consistent with significantly reduced π-bonding. Double occupation in the Mo^{IV} low-spin form would reduce the bond order to 1.

This simple bonding model is consistent with the properties of [Mo^{V}OSL]$^-$ described above and particularly with the evidence (points i and ii above) for a longer molybdenum–thio distance. It also rationalizes the observation of conjugate acid and base species in XnO. The Mo and S valence orbitals are matched so that occupation of the MoS π-antibonding orbital progressively increases the basic character of the thio ligand. The basic form only is seen for Mo^{VI}, the acid form only for Mo^{IV}, and both forms for Mo^{V}. Consequently, a specific mechanism is provided for the correlated electron–proton transfer property of oxomolybdenum enzymes and for XnO in particular. This point was first specifically discussed in the context of molybdenum enzymes by Stiefel.[78]

It is of interest to note that the enzymes which feature MoOS centers act upon *covalent* CH bonds while those that feature MoO$_2$ centers do not. It would appear that the extra base strength associated with the reduced MoOS centers is needed for activation of CH bonds. In another context, very significant participation of ligand cysteinyl sulfur (or selenium) in active site valence orbitals has been inferred recently in blue copper proteins[79] and in [NiFe]hydrogenases.[80]

"Strongly Coupled" Protons. The XnO signals exhibit A(^{1}H) that are nearly isotropic (Table I). This contrasts with the significant anisotropy in [MoO(XH)L] (X = O, S) (Table II), which was discussed above in terms of the presence of both direct and indirect dipolar coupling. It would seem that, in the enzyme, either (1) the direct and indirect anisotropic components essentially cancel or (2) the MoXH bond angles are larger, increasing *r*(MoH) and decreasing the direct component. It is entirely possible that steric constraints within the active site lead to the second situation.

Nature of the Rapid Type 2 and Alloxanthine Signals. The Rapid Type 2 signal represents an apparently noncatalytically active center that is favored under basic conditions.[12,38] The observed **g**, A(^{95}Mo), and A(^{33}S) closely follow those of the Rapid Type 1 signal (Tables I and III), confirming very similar ligand environments. Rapid Type 2 exhibits a second *strongly* coupled proton (Table I) and ^{17}O coupling similar in magnitude to that observed in the Rapid Type 1 and Slow signals.[54] This data is consistent with an OH ligand competing with bound product, OR, formed by turnover of substrate RH: Rapid Type 1, Mo^{V}O(SH)(OR); Rapid Type 2, Mo^{V}O(SH)(OH).

The alloxanthine signal features **g** and A(^{33}S) matrices closely related to those of the Very Rapid signal (Tables I and III). Consequently, a [Mo^{V}OS] center is present in both. The alloxanthine signal also exhibits ^{14}N coupling, assigned to bound substrate, NR′, but not the ^{17}O couplings observed in the Very Rapid signal.[74,75] Consequently, the two signals can be assigned to the following centers: Very Rapid, Mo^{V}OS(OR); Inhibited alloxanthine, Mo^{V}OS(NR′).

EXAFS data on the Mo^{IV} form of the alloxanthine complex[9] are consistent with the protonated structure Mo^{IV}O(SH)(NR′). However, the assignment of bound product OR in both the Very Rapid and Rapid Type 1 signals is less certain given the remarkable difference in the anisotropy of the ^{17}O coupling in the two cases.[75,76] The magnitude of ^{17}O coupling for an OR group bound cis to an oxo ligand appears to vary significantly with its detailed environment.[17] Further aspects can be addressed by detailed examination of ^{17}O coupling in the present analogue complexes, and this is currently in progress.

Catalysis at the Molybdenum Site in XnO. The present work allows some consolidation of the current understanding[5,11,16] of

(74) Hawkes, T.; George, G. N.; Bray, R. C. *Biochem. J.* **1984**, *218*, 961–968.
(75) Gutteridge, S.; Bray, R. C. *Biochem. J.* **1980**, *189*, 615–623.
(76) Morpeth, F. F.; George, G. N.; Bray, R. C. *Biochem. J.* **1984**, *220*, 253–260.
(77) Combariza, J. E.; Enemark, J. H.; Barfield, M.; Facelli, J. C. *J. Am. Chem. Soc.* **1989**, *111*, 7621–7622.
(78) Stiefel, E. I. *Proc. Natl. Acad. Sci. U.S.A.* **1973**, *70*, 988–992.
(79) Werst, M. M.; Davoust, C. E.; Hoffman, B. M. *J. Am. Chem. Soc.* **1991**, *113*, 1533–1538.
(80) Eidness, M. K.; Scott, R. A.; Prickril, B. C.; DerVartanian, D. V.; Legall, J.; Moura, I.; Moura, J. J. G.; Peck, H. D., Jr. *Proc. Natl. Acad. Sci. U.S.A.* **1989**, *86*, 147–151.

Scheme II. Proposed Catalytic Cycle for the Molybdenum Site in XnO

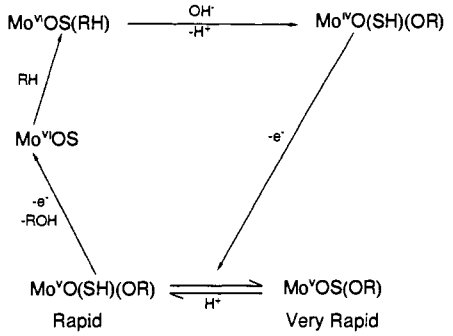

the minimal catalytic cycle at the Mo site of XnO (Scheme II). There is some uncertainty[11] as to whether the Very Rapid center is on the main catalytic pathway and detailed observations are substrate-dependent. However, given the simple acid-base relationship between the $Mo^{V}OS($ (Very Rapid) and $Mo^{V}O(SH)$ (Rapid) found in the present work, and the possible presence of molybdenum-bound product OR modulating the system, a substrate dependence is unsurprising. The single equation in Scheme II describing the Mo^{VI} to Mo^{IV} redox event masks a number of primary steps. These include electron transfer from substrate to molybdenum, proton transfer from substrate to thio sulfur, and an apparent oxygen atom transfer from oxo ligand to substrate[4] with replacement of the former from water. While a specific mechanism for the electron-proton transfer is addressed in the present work, the existing analogue species containing quadridentate ligand L cannot probe potential oxygen atom transfer to substrate as a model substrate site is not available. Tridentate ligands that both allow observation of $Mo^{V}OX$ and $Mo^{V}O(XH)$ centers (X = O, S) and provide a model substrate site are currently under development.[81]

Acknowledgment. A.G.W. thanks the Australian Research Council for financial support. J.T.S. acknowledges support from NIH Grant GM 08347. Professor J. H. Enemark is thanked for stimulating discussion.

(81) Xiao, Z.; Laughlin, L.; Young, C. G.; Enemark, J. H.; Wedd, A. G. Work in progress.

Nuclear Quadrupole Resonance Study of ^{51}V in Metavanadates†

D. Mao, P. J. Bray,* and G. L. Petersen

Contribution from the Department of Physics, Brown University, Providence, Rhode Island 02912.
Received November 23, 1990

Abstract: Pure nuclear quadrupole resonance (NQR) studies of ^{51}V in several metavanadates have been performed at both room temperature and liquid nitrogen temperature. Values of the quadrupole interaction parameters (Q_{cc}'s and η's) in these compounds were obtained, which are more than an order of magnitude more accurate than those obtainable from NMR studies. Multiquantum transitions have been found in some cases. A sensitive NQR spectrometer was constructed for this study with a Robinson-type oscillator, a bi-symmetric square wave magnetic field modulator, and a data acquisition system based on an IBM PC/XT computer.

Introduction

The interaction between a nucleus (spin 1 or greater) possessing an electrical quadrupole moment and the electric field gradient (EFG) at the nuclear site provides important information about the chemical bonding and environment of the atom containing the nucleus under investigation. It has been proven to be a valuable probe in the study of the structure and chemistry of solid materials.[1,2] A conventional way to obtain quadrupole interaction parameters is through comparison of experimental NMR spectra with computer-stimulated spectra that include the effects of the quadrupole interaction.[3-8] But the quadrupole interaction parameters obtained by this method are generally not of high accuracy because of the following: (1) the second-order NMR line shape of the central ($m = +^1/_2 \leftrightarrow m = -^1/_2$) transition of half-integer spin nuclei is not very sensitive to changes in quadrupole interaction parmeters of as much as 5% or more;[8] (2) when the chemical shift interaction and the quadrupole interaction are both present and comparable in magnitude, the NMR line shapes are very complicated and difficult to analyze; (3) in the computer simulation of NMR line shapes, there is a possible systematic error present in the assumption that the principal axes of the chemical shift tensor and the EFG tensor coincide with each other, which is not necessarily true;[9] and (4) in the presence of large quadrupole interactions, the NMR spectra are usually too wide (say 200 kHz) to be excited homogeneously due to the limitation of the RF power of the pulsed NMR spectrometer. On the other hand, pure nuclear quadrupole resonance provides a direct and accurate method to measure the quadrupole interaction parameters. Recently, Bray and Gravina[10] have studied ^{11}B and ^{10}B NQR in crystalline and vitreous B_2O_3 and some borate compounds and glasses in the frequency region from 250 kHz to 2 MHz with a sensitive Robinson oscillator.[11] Their results show that ^{11}B and ^{10}B NQR spectroscopy can distinguish responses from different BO_3 structural units in borate crystals and glasses.

† Research supported by the National Science Foundation through NSF Grant No. DMR-8920532.

(1) Cohen, M. H. *Phys. Rev.* **1954**, *96*, 1278.
(2) Weiss, A. *Adv. Nucl. Quadrupole Reson.* **1972**, *1*, 1.
(3) Abragam, A. *The Principles of Nuclear Magnetism*; Oxford University Press: London, 1961.
(4) Slichter, C. P. *Principles of Magnetic Resonance*; Harper and Row Publishers, Inc.: New York, 1963.
(5) Cohen, M. H.; Reif, F. *Solid State Physics*; Academic Press Inc.: New York, 1957; Vol. 5.
(6) Stauss, C. H. *J. Chem. Phys.* **1964**, *40*, 1988.
(7) Narita, K.; Umeda, J.; Kusumoto, H. *J. Chem. Phys.* **1966**, *44*, 2719.
(8) Taylor, P. C.; Baugher, J. F.; Kriz, H. M. *Chem. Rev.* **1975**, *75*(2), 203.
(9) Baugher, J. F.; Taylor, P. C.; Bray, P. J. *J. Chem. Phys.* **1969**, *50*(11), 4914.
(10) Bray, P. J.; Gravina, S. J. *Proc. XVth Int. Congr. Glass, Leningrad* **1989**, *1a*, 63.
(11) Robinson, F. N. H. *J. Phys. E: Sci. Instrum.* **1982**, *15*, 814.

0002-7863/91/1513-6812$02.50/0